DOI: 10.1002/cphc.200700839

Organelle Tracking in a Living Cell with Microsecond Time Resolution and Nanometer Spatial Precision

Xiaolin Nan, Peter A. Sims, and X. Sunney Xie*[a]

The study of cellular processes such as organelle transport often demands particle tracking with microsecond time-resolution and nanometer spatial precision, posing significant challenges to existing tracking methods. Here, we have developed a novel strategy for two-dimensional tracking of gold nanoparticles (GNPs) with 25 μs time resolution and ~1.5 nm spatial precision, by using a quadrant photodiode to record the positions of GNPs in an objective-type dark-field microscope. In combination with a feedback loop, this technique records long, high time-resolution and spatial precision trajectories of endocytosed GNPs transported by the molecular motors kinesin and dynein in a living cell. In the full range of organelle velocities (0–8 $\mu m s^{-1}$), we clearly resolve the individual 8 nm steps of cargoes carried by kinesin, and the 8, 12, 16, 20, and 24 nm steps of those carried by dynein. These experiments yield new information about molecular motor stepping in living cells.

Introduction

Particle tracking is an important tool for studying cellular processes that involve molecular motions. In a particle tracking experiment,[1,2] the information obtainable from the acquired trajectories is often determined by the time resolution (i.e. the sampling rate) and spatial precision (precision in determining the particle location). Nanometer precision can be achieved for isolated particles[3] and even for single fluorophores[4] so long as the signal to noise ratio is high enough.[5] However, few existing particle tracking methods offer submillisecond time-resolution with nanometer precision in living cells, which is necessary for probing many cellular processes.

For example, the molecular motors kinesin and dynein carry organelles along microtubules in cells[6] with reported velocities as high as 10 $\mu m s^{-1}$,[7,8] possibly in discrete steps as small as 8 nm.[8–10] This means that the waiting time between the motor steps is, on average, only 800 μs at the highest velocity. Due to the randomness of stepping events, two successive 8 nm steps can be even more closely (e.g. 100 μs) spaced, making them indistinguishable from a single 16 nm step. This is particularly true in the presence of diffusive organelle motions (see Supporting Information Figure 1). To adequately evaluate the stepping behavior of these molecular motors in living cells, one has to be able to track their movements with a time resolution much better than 800 μs and simultaneously, a spatial precision much better than 8 nm.

Attempts to observe the individual steps of microtubule motor-driven organelles in vivo have been made with GFP-labeled peroxisomes[9] and endocytosed quantum dots[8,10] with fluorescence microscopy, as well as melanosomes imaged with bright field/DIC microscopy,[11] all with 1–2 nm spatial precision. However, the best time resolution in these studies was on the order of 1 ms. The insufficient time resolution resulted in discrepancies in the reported step sizes,[8–11] leaving the most fundamental questions about motor stepping in vivo largely unanswered.

Herein we present a novel particle tracking scheme with 25 μs time resolution and ~1.5 nm spatial precision in live cells. This high time-resolution and spatial precision are made possible by the strong scattering signal from gold nanoparticles (GNPs) imaged with dark-field microscopy. We employed an efficient detection scheme and a quadrant photodiode (QPD) to record the positions of GNPs in an objective-type dark-field microscope. By integrating this tracking scheme with a positional feedback loop, we record long (tens of microns), high time-resolution and spatial precision trajectories of endocytosed GNPs actively transported by kinesin and dynein. These trajectories reveal detailed information about motor stepping in vivo.

Results and Discussion

Objective-Type Dark-Field Microscopy

In the objective-type dark-field microscope (ODFM, Figure 1a), the same, high numerical aperture objective delivers a diagonal illumination laser beam to the field of view and efficiently collects the light scattered by the GNPs (Figure 1a). With a field stop (iris) in the detection path, one can separate the scattered light from reflected, incident light and obtain clean, dark-field images.

Our setup is a variation of a previously described ODFM[12,13] with two major improvements. First, we implemented asym-

[a] *Dr. X. Nan, P. A. Sims, Prof. X. S. Xie*
Department of Chemistry and Chemical Biology
Harvard University
12 Oxford Street, Cambridge, MA 02138 (USA)
Fax: (+1) 617 496 8709
E-mail: xie@chemistry.harvard.edu

Supporting information for this article is available on the WWW under http://www.chemphyschem.org or from the author.

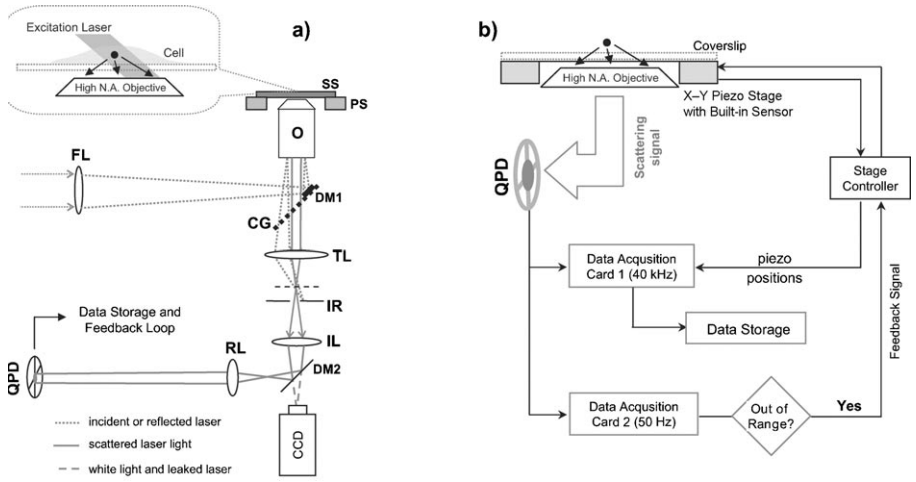

Figure 1. a) ODFM set-up and b) feedback loop, see Experimental Section for details.

metric dark-field illumination by projecting a single round, focused beam onto the back aperture of the objective. An asymmetric illumination scheme similar to ours was used in an in vitro study of kinesin.[14] Our setup is simple compared to the symmetric illumination produced by an axicon because we avoid using diffractive or diffusive elements.[12,13] Second, a small mirror mounted on clear glass (DM1 in Figure 1a) is used to reflect the incident beam into the objective, allowing efficient reflection of the incident beam as well as efficient transmission of scattered signal. Compared with the use of a beam splitter as in previous reports,[12,13] we can obtain the same amount of signal with only half of the illumination power on the sample.

We use 100–150 nm diameter GNPs not only because they are comparable in size to cellular organelles, but also because their signal in the cytoplasm is strong enough (150 nW per particle) for high-speed tracking with 532 nm illumination at a moderate power density of 30–50 $\mu W\,\mu m^{-2}$ (see Supporting Information, Figure 2).[15,16] This signal is about 200–1000 times that of QD-aggregates.[8] An even lower illumination power density can be used with a 546 nm laser, which is closer to the plasmon resonance of 100–150 nm GNPs.[15,16] By projecting the image of individual GNPs onto a QPD detector,[17] we record the positions of GNPs with 25 μs time-resolution and 1–2 nm spatial precision.

We calibrated the QPD by using the setup to detect 10 and 20 nm artificial steps of 150 nm GNPs immobilized on a coverslip driven by a piezo stage (see Supporting Information, Figure 3). We note that the 25 μs time resolution is limited by the size of the GNPs (100–150 nm) that we used. With slightly larger GNPs, for example, those 200–250 nm in diameter, the signal is 3–5 fold stronger and the time resolution can be further increased to about 5–10 μs.

Feedback Loop for Long-Range Particle Tracking

Because the linear tracking range of our QPD detector (~150 nm off-center) is much shorter than the typical run lengths of microtubule motor-driven organelles (several microns),[6] we implemented a feedback system that uses a two-dimensional (*x*–*y*) piezo stage to move the sample (if necessary) every 20 ms such that the particle being followed remains within the tracking range of the QPD (Figure 1b). Consequently, the *x*–*y* position readings from the QPD circuitry reflect the position of the particle relative to the QPD that does not move. Meanwhile, the adjustment made by the piezo stage is recorded by a high precision, high bandwidth position sensor built in the piezo stage. By combining the readings of the QPD and the piezo stage position sensor, the actual position of the particle being tracked can be easily recovered. With this feedback loop, the tracking distance is limited only by the travel range of the piezo stage (~150 μm). Although we have only implemented 2D particle tracking in vivo, our system is readily adaptable to 3D tracking, for example, with the approach demonstrated recently in vitro by Cang et al.[18]

Tracking of Organelles Moving Along Microtubules

GNPs coated with human fibroblast growth factor are introduced into human lung cancer (A549) cells by incubation overnight. Following endocytosis, the GNPs are mostly enclosed in lysosomal vesicles as evidenced by immunofluorescence (see Supporting Information, Figure 4) and electron microscopy (Supporting Information, Figure 5). The GNPs appear as individual bright spots under the dark-field microscope (Figure 2a).

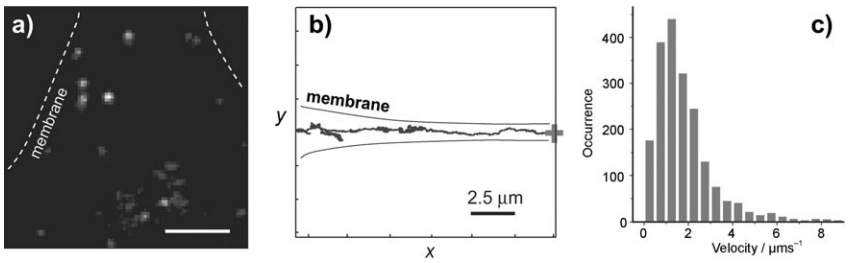

Figure 2. Tracking GNPs in live A549 cells. a) Dark-field image of endocytosed GNPs inside an A549 cell. The bright dots are the organelles containing GNPs, and the dashed lines mark the cell membrane. Scale bar: 5 μm; b) A ~17 μm long *x*–*y* trajectory (grey line) obtained with the tracking system on an organelle moving in a long protrusion of an A549 cell, from the end of a cell protrusion (+) towards the cell center. The black lines mark the cellular membrane; c) Velocity distribution in the first 10 s along the trajectory in (b). The broad distribution of in vivo velocity (0–8 $\mu m\,s^{-1}$) has an average around 1.6 $\mu m\,s^{-1}$.

Similar to the endocytosed QDs,[8] these GNP-containing vesicles often made rapid movements along linear tracks, indicative of active transport by molecular motors. Consistent with our control experiments (data not shown), previous reports have identified that the kinesin motors transport lysosomes (or late endosomes) towards the cell membrane (outward movements),[19,20] whereas dynein transports cargoes in the opposite direction (inward movements).[21–23]

In conducting a tracking experiment, we first place a particle of interest (visually identified on the CCD camera) in the QPD field of view by manually adjusting the piezo stage. The feedback loop is then engaged to keep the image of the particle on the QPD during active transport (see Supporting Information Video and Supporting Information Figure 6). We could easily record long trajectories of GNP-containing vesicles moving along microtubules, often in the range of 10–30 μm (Figure 2b), allowing us to determine the directionality of the active transport, that is, inward or outward.

We measured the average velocities in both the inward and outward movements of these GNP-containing vesicles to be around 1–2 $\mu m\,s^{-1}$ when using 150 nm GNPs with the velocity histogram shown in Figure 2c. The fastest movements can be up to ~8 $\mu m\,s^{-1}$ within short (5 ms) time windows.

Stepwise Movements in Kinesin and Dynein Trajectories

The high time-resolution and spatial precision of our tracking system enabled us to resolve individual steps and to determine the step size for the entire range of cargo velocities (0–8 $\mu m\,s^{-1}$). For instance, even at a velocity of ~8 $\mu m\,s^{-1}$ (1 ms per 8 nm step), there are still 40 position points on average to define a single 8 nm step.

A few representative trajectories of cargoes travelling outward or inward are shown in Figures 3a and b, respectively. The stepwise movements are not only evident in the displacement trajectories but also in the *x*–*y* position plots (Figure 3c; see also Supporting Information, Figure 7), appeared as small "clusters" of positions, a result of diffusive motions of the cargo during the waiting time between the steps. We note that a small fraction of our trajectories do not exhibit clear, stepwise movements possibly due to loose coupling between the vesicle and the GNP.

The histograms of step sizes in the kinesin and dynein directions are shown in Figures 3d and e, respectively. A comparison between Figures 3a and d and Figures 3b and e clearly shows that, while cargoes carried by kinesin exhibit exclusively 8 nm steps, regardless of the velocity, those carried by dynein exhibit both 8 nm and larger step sizes at all organelle velocities. We also notice that in dynein trajectories, the large steps often occur consecutively, as suggested by trajectories shown in Figure 3b and the conditional histogram in Figure 4a, which shows that a large ($\geq$12 nm) step tends to be followed by another large step.

Noticeably, Figure 4a shows distinct peaks around 8, 12, 16, 20, and 24 nm. While some in vitro studies[24,25] suggest that dynein can take 8, 16, and 24 nm steps, the 12 and 20 nm steps that are evident in our histogram and displacement trajectories (Figure 4b) have not been reported previously. Among many possible explanations, these 12 and 20 nm steps could be attributed to actual step sizes of dynein (Figure 4c), or to multiple dyneins carrying the same cargo.[7,26] More studies are needed to fully explain these interesting observations.

In addition to step size, other aspects of motor stepping in vivo can now be studied in fine detail. For example, the kinesin and dynein steps appeared as abrupt "jumps" in displacement

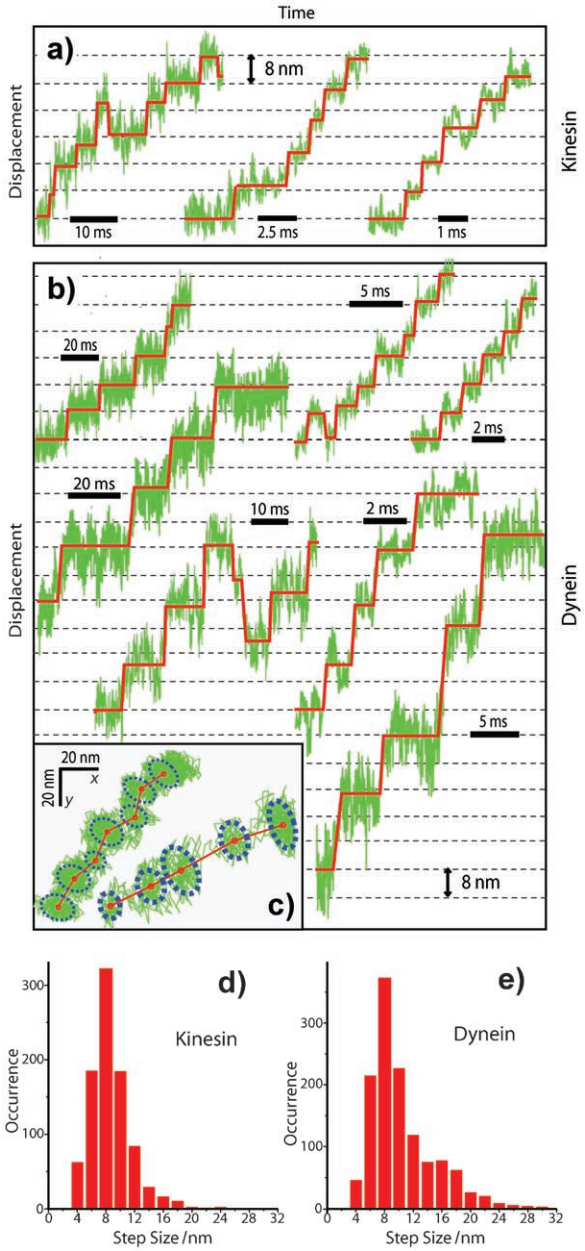

Figure 3. Stepwise movements of organelles. a) Displacement trajectories of organelles carried by kinesin; b) Displacement trajectories of organelles carried by dynein. The green lines are the raw trajectories and the red lines outline the steps (see the Experimental Section for details on step-finding); c) Position (*x*–*y*) plots of organelles carried by dynein, showing small clusters of GNP positions due to the diffusion of the organelle during waiting periods between steps; d) Step-size distribution in the kinesin trajectories, showing a single peak at 8 nm; e) Step-size distribution in the dynein trajectories, showing a wide distribution of step sizes from 8 nm to ~24 nm.

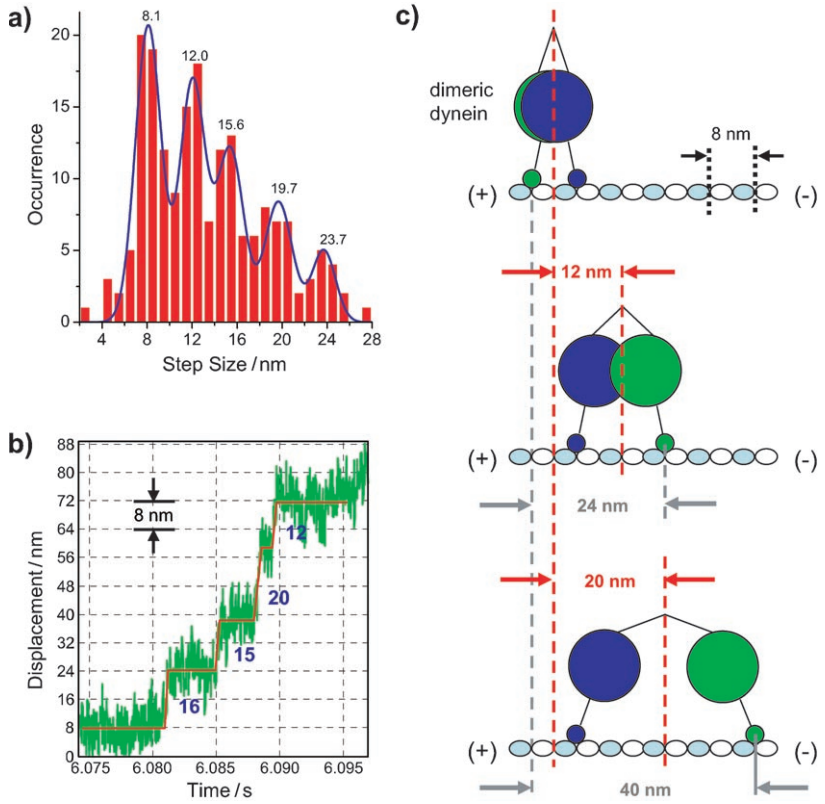

Figure 4. 12 and 20 nm steps of dynein in vivo. a) Histogram showing the size of the steps immediately following a large ($\geq$12 nm) step, exhibiting multiple peaks near 8, 12, 16, 20, and 24 nm. The blue curve is the fitting to 5 Gaussian distributions. b) Segment of a displacement trajectory showing both 12 and 20 nm steps following two consecutive 16 nm steps; c) Possible scheme for the 12 and 20 nm steps of dynein, based on a previously proposed "alternating shuffle" model[25] for dynein stepping. The filled and void ellipses stand for the α and β tubulin subunits of the microtubules. In the starting configuration (top panel) the two heads are 8 nm apart. In the middle panel, the green (rear) head moves forward (to the minus end of microtubules) and binds to another site which is 24 nm away from its original position (gray, dashed line), resulting in a 12 nm shift of the center of mass of the dimer (dynein). Similarly, a 20 nm steps is achieved by the green head taking a forward head step of 40 nm (bottom panel, gray, dashed line). By binding to other available motor binding sites, 8, 16, 24,…, nm steps are achieved. The structures are drawn roughly to scale.

trajectories in previous in vivo experiments.[8–10] In the current experiment, however, these steps are found to be gradual rises occurring on the 100 μs to few millisecond timescale (Figures 5a and b). In comparison, the rise time for kinesin steps in vitro[14,27,28] is typically 20–50 μs. Among possible factors, local mechanical properties of the cytoplasm and the stiffness of the neck-linker likely determine the rise time.[14,27,28] A more detailed analysis of the rise time of the steps is currently underway, which should provide useful information about the mechanics of motor steps in vivo.

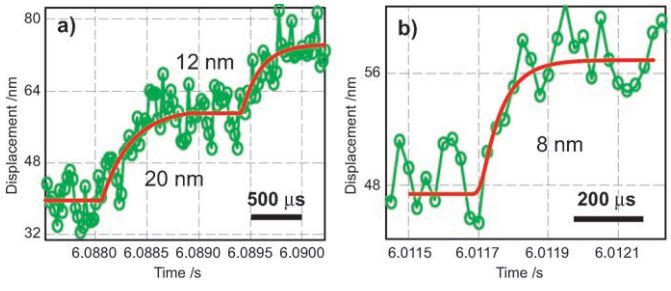

Figure 5. Rising phase of motor steps in vivo. a) Segment of a displacement trajectory with a 20 nm step and a 12 nm step, showing rise times of ~500 and ~250 μs, respectively; b) Different segment showing an 8 nm step with a rising time of ~120 μs. The connected, green circles are the raw displacement trajectory, and the red lines are fittings to steps intercepted with single exponential rising phases.[14]

Conclusions

We developed the described particle tracking system to address a compelling biological problem. While recent experiments have demonstrated the ability to resolve individual steps of kinesin and dynein in vivo, the steps were only resolved at slow velocities (up to ~2 μm s^{-1}) mainly due to the limited time-resolution. The step sizes of dynein reported in these studies are different from each other. Fundamental questions about the stepping behavior of dynein in vivo, therefore, remain largely unanswered. Here, with microsecond time-resolution and nanometer spatial precision, individual steps of both kinesin and dynein can now be clearly resolved at the full range in vivo velocities (0–8 μm s^{-1}). Our data prove that while cargoes carried by kinesin exhibit only 8 nm steps, those carried by dynein exhibit both 8 nm and larger (12, 16, 20, and 24 nm) steps. Although the understanding of how motors work individually and collectively in vitro and in vivo is far from complete, the high resolution measurements required by this complex problem is afforded by the technique. We believe that the technique facilitates this quest and anticipate that it will be applied to studies of other cellular processes.

Experimental Section

Dark-Field Microscopy and Particle Tracking: The objective-type dark-field microscope was based on a previous scheme[12] with modifications. Light from a green laser (532 nm, Verdi V5, Coherent) was coupled into a single mode fiber and reflected to the back of the microscope (TE-300, Nikon) that sits on a separate optical bench. The output from the fiber was collimated, expanded, and then focused onto the back aperture of a high N.A. objective (oil, 60x, NA1.45, Nikon) with an f=400 mm lens (FL). Dark-field il-

lumination is achieved by shifting the focused laser beam off-center on the objective back aperture, resulting in a diagonally collimated beam coming out of the objective. For the reflector, we glued a small, round mirror (~5 mm in diameter) on a piece of clear BK-7 glass (mounted in the dichroic cube at 45°) at the spot where the incident, focusing beam strikes the glass. By doing so, all of the incident light can be reflected into the objective and ~90% of the scattering signal collected by the objective reaches the detector.

Light scattered by the particles inside the cell and reflected at interfaces was collected by the same objective (O). Due to differences in focusing properties, scattered light (signal, divergent in focus) and reflected light (background, collimated in focus) formed images at different places after the tube lens (TL). An iris (IR) was placed at the image plane of background (dashed line above the image plane for the signal), thereby rejecting the background. The scattering signal had a different image plane and passed through the center of the iris. The resulting image was then magnified by an aspheric lens (RL) after reflection on DM2 and projected onto a quadrant photodiode (QPD, 58-278, Edmund Optics, NJ). With a moderate laser excitation density (30–50 $\mu W\,\mu m^{-2}$), the signal from individual gold nanoparticles (GNPs, 150 nm in diameter) are typically ~150 nW, allowing for the QPD to operate with 25 μs time resolution (40 kHz bandwidth, −3 dB) and to detect the position of the beads with ~1 nm spatial precision. The bandwidth of the QPD detector and amplifier circuit was verified by clearly resolving individual laser pulses from an 80 MHz Tsunami (Spectra Physics) pulse-picked to 40 kHz. We calibrated the QPD by recording the 10 and 20 nm steps of static 150 nm GNPs (Figure 1c) or 200 nm poly-styrene beads (Supporting Information Figure 3) on a coverslip driven by a piezo stage (P-517.3CL, Physik Instrumente, MA) as described previously.

We also collect the leak-through (~2%) of the signal through one of the mirrors (DM2 in Figure 1a) with a CCD camera, on which a superimposed bright field image of the entire cell can be viewed. We identified a small region on the CCD that corresponds to the active area of QPD by looking at a static GNP on a coverslip with both devices at the same time. Thereafter, to bring the image of a particle onto the QPD quickly, we could simply move its dark-field image on the CCD into the pre-defined region by manually adjusting the DC offset on the piezo stage controller.

On a computer equipped with a data acquisition card (DAQ2), readings of the positions of GNPs from the QPD were sampled every 20 ms to determine if the image of the particle was off center on the QPD by a certain distance in either dimension (typically 75–120 nm). If so, a feedback signal is given to the piezo stage in order to re-center the image on the QPD. Simultaneously, the signals from the QPD amplifier and readings from the built-in piezo position sensors from the stage controller (E-509.C3, Physik Instrumente, MA, modified for high bandwidth), were sampled on another computer at 40 kHz with a Ni-DAQ card (DAQ1, PCI-6143, National Instruments, TX) and stored without filtering. The readings were then recombined to recover the absolute coordinates of the particle. All of the data acquisition and feedback scripts were written in LabView 7.0 (National Instruments, TX).

Gold Nanoparticle and Growth Factor Conjugates: Gold nanoparticles (GNPs, 100, 150, and 200 nm) were purchased from Corpusclular, Inc. (NY). Human fibroblast growth factor (hFGF, F0291) was purchased from Sigma. To conjugate hFGF to GNPs, we used a previously developed procedure.[29] Briefly, to 100 μL of GNPs we added ~4 μL of hFGF (0.2 $\mu g\,\mu L^{-1}$) and 5 μL of 0.1% poly-ethylene glycol (PEG, MW = 10000, Sigma P6667) and incubated for an hour. The GNPs were collected by mild centrifugation on a bench-top mini spinner (VWR C1213, fast centrifugation should be avoided), and re-suspended in 1x PBS buffer (pH 7.4). GNP conjugates were freshly prepared for each experiment.

Cell Culture and Uptake of GNPs: A549 (human lung cancer) cells were obtained from American type cell culture (ATCC), cultured in DMEM with 10% FBS (ATCC) under humidified 5% CO_2 at 37°C. Cells were seeded onto Delta-T dishes (Bioptechs, NJ) with #1.5 glass coverslip bottoms at least 24 h before adding GNPs. During imaging experiments, the temperature of the culture was maintained at 37°C with a temperature controller (Bioptechs 0420-4-03). We introduced GNPs into the cells by adding 2–5 μL of GNP-hFGF conjugates to each Delta-T dish containing ~1.5 mL medium and incubating overnight. With this small dose, the average number of GNPs per cell is only 10–20.

Data Analysis: All data analysis was performed with home-written MatLab (Mathworks, MA) scripts. The *x*–*y* trajectories from in vivo experiments are often curved, and were first divided into relatively straight segments for calculation of displacement trajectories. The trajectories were analyzed using the same method as in our previous work[8] (Supporting Information, Figure 8), with similar results to another recently developed step-finding algorithm[25,30] (Supporting Information, Figure 9).

Acknowledgements

This work is supported by an NIH grant P20 GM072069 and an NIH Director's Pioneer Award to X.S.X. P.A.S. is supported by an NSF graduate research fellowship. We thank Drs. Brian English, Conor Evans, Feruz Ganikhanov and David Ward for their help with programming and instrumentation, Drs. Charles Schroeder and Guobin Luo for critical readings of the manuscript, and Dr. Paul Blainey and Sangjin Kim for helpful discussions.

Keywords: dark-field microscopy · gold nanoparticles · motor protein · organelle transport · particle tracking

[1] A. Kusumi, C. Nakada, K. Ritchie, K. Murase, K. Suzuki, H. Murakoshi, R. S. Kasai, J. Kondo, T. Fujiwara, *Annu. Rev. Biophys. Biomol. Struct.* **2005**, *34*, 351–378.
[2] M. J. Saxton, K. Jacobson, *Annu. Rev. Biophys. Biomol. Struct.* **1997**, *26*, 373–399.
[3] J. Gelles, B. J. Schnapp, M. P. Sheetz, *Nature* **1988**, *331*, 450–453.
[4] A. Yildiz, J. N. Forkey, S. A. McKinney, T. Ha, Y. E. Goldman, P. R. Selvin, *Science* **2003**, *300*, 2061–2065.
[5] R. E. Thompson, D. R. Larson, W. W. Webb, *Biophys. J.* **2002**, *82*, 2775–2783.
[6] M. Schliwa, G. Woehlke, *Nature* **2003**, *422*, 759–765.
[7] A. Ashkin, K. Schutze, J. M. Dziedzic, U. Euteneuer, M. Schliwa, *Nature* **1990**, *348*, 346–348.
[8] X. Nan, P. A. Sims, P. Chen, X. S. Xie, *J. Phys. Chem. B* **2005**, *109*, 24220–24224.
[9] C. Kural, H. Kim, S. Syed, G. Goshima, V. I. Gelfand, P. R. Selvin, *Science* **2005**, *308*, 1469–1472.
[10] T. M. Watanabe, H. Higuchi, *Biophys. J.* **2007**, *92*, 4109–4120.
[11] C. Kural, A. S. Serpinskaya, Y. H. Chou, R. D. Goldman, V. I. Gelfand, P. R. Selvin, *Proc. Natl. Acad. Sci. USA* **2007**, *104*, 5378–5382.
[12] I. Braslavsky, R. Amit, B. M. Ali, O. Gileadi, A. B. Oppenheim, J. Stavans, *Appl. Opt.* **2001**, *40*, 5650–5657.
[13] S. Kim, P. C. Blainey, C. M. Schroeder, X. S. Xie, *Nat. Methods* **2007**, *4*, 397–399.
[14] M. Nishiyama, E. Muto, Y. Inoue, T. Yanagida, H. Higuchi, *Nat. Cell Biol.* **2001**, *3*, 425–428.

[15] P. K. Jain, K. S. Lee, I. H. El-Sayed, M. A. El-Sayed, *J. Phys. Chem. B* **2006**, *110*, 7238–7248.
[16] M. A. van Dijk, A. L. Tchebotareva, M. Orrit, M. Lippitz, S. Berciaud, D. Lasne, L. Cognet, B. Lounis, *Phys. Chem. Chem. Phys.* **2006**, *8*, 3486–3495.
[17] K. C. Neuman, S. M. Block, *Rev. Sci. Instrum.* **2004**, *75*, 2787–2809.
[18] H. Cang, C. M. Wong, C. S. Xu, A. H. Rizvi, H. Yang, *Appl. Phys. Lett.* **2007**, *88*, 223 901.
[19] J. K. Burkhardt, C. J. Echeverri, T. Nilsson, R. B. Vallee, *J. Cell Biol.* **1997**, *139*, 469–484.
[20] C. Valetti, D. M. Wetzel, M. Schrader, M. J. Hasbani, S. R. Gill, T. E. Kreis, T. A. Schroer, *Mol. Biol. Cell* **1999**, *10*, 4107–4120.
[21] N. Hirokawa, *Science* **1998**, *279*, 519–526.
[22] P. J. Hollenbeck, J. A. Swanson, *Nature* **1990**, *346*, 864–866.
[23] T. Nakata, N. Hirokawa, *J. Cell Biol.* **1995**, *131*, 1039–1053.
[24] R. Mallik, B. C. Carter, S. A. Lex, S. J. King, S. P. Gross, *Nature* **2004**, *427*, 649–652.
[25] S. L. Reck-Peterson, A. Yildiz, A. P. Carter, A. Gennerich, N. Zhang, R. D. Vale, *Cell* **2006**, *126*, 335–348.
[26] D. B. Hill, M. J. Plaza, K. Bonin, G. Holzwarth, *Eur. Biophys. J.* **2004**, *33*, 623–632.
[27] L. Busoni, A. Dupont, C. Symonds, J. Prost, G. Cappello, *J. Phys. Condens. Matter* **2006**, *18*, S1957–S1966.
[28] N. J. Carter, R. A. Cross, *Nature* **2005**, *435*, 308–312.
[29] K. Sokolov, M. Follen, J. Aaron, I. Pavlova, A. Malpica, R. Lotan, R. Richards-Kortum, *Cancer Res.* **2003**, *63*, 1999–2004.
[30] J. W. Kerssemakers, E. L. Munteanu, L. Laan, T. L. Noetzel, M. E. Janson, M. Dogterom, *Nature* **2006**, *442*, 709–712.

Received: December 17, 2007

